JAE-YUN KIM[1], SANG-GYU KIM[1], BYOUNGCHUL HWANG[1*]

INVESTIGATION OF HYDROGEN EMBRITTLEMENT OF HAYNES 617 AND HASTELLOY X ALLOYS USING ELECTROCHEMICAL HYDROGEN CHARGING

This study explores the hydrogen embrittlement behaviour of two Ni-based superalloys using electrochemical hydrogen charging. Two types of tensile specimens with different geometry for the Haynes 617 and Hastelloy X alloys were electrochemically hydrogen-charged, and then a slow strain rate test was conducted to investigate the hydrogen embrittlement behaviour. Unlike the ASTM standard specimens, two-step dog-bone specimens with a higher surface-area-to-volume ratio showed higher sensitivity to hydrogen embrittlement because hydrogen atoms are distributed mostly on the surface area. On the other hand, the Haynes 617 alloy had a lower hydrogen embrittlement resistance than that of the Hastelloy X alloy due to its relatively large grain size and the presence of precipitates at grain boundaries. The Haynes 617 alloy primarily showed an intergranular fracture mode with cracks from the slip band, whereas the Hastelloy X alloy exhibited a combination of transgranular and intergranular fracture behavior under hydrogen-charged conditions.

Keywords: Ni-based superalloy; hydrogen embrittlement; specimen geometry; electrochemical hydrogen charging; slow strain-rate test (SSRT)

1. Introduction

Hydrogen, as a carbon-free energy carrier, is expected to play a major role in renewable energy sources for addressing global warming. Of the conventional fossil-fuel power generation technologies, gas turbine power generation is regarded as one of the cleanest energy systems, but hydrocarbon-based fuels still generate significant CO_2 emissions [1-3]. Using hydrogen instead of hydrocarbon-based fuels for gas turbines can greatly reduce or eliminate CO_2 emissions. However, gas turbine combustion systems must be redesigned to use hydrogen as fuel because hydrogen combustion affects the high-temperature components of gas turbines [4-6]. Therefore, it is necessary to consider not only the combustion characteristics but also the effects of hydrogen on the reliability of materials and components used in gas turbine because hydrogen can affect material properties such as hydrogen embrittlement [7,8].

Ni-based alloys have good strength at high temperature and high resistance to creep, making them compatible materials for gas turbines [9,10]. In fact, using hydrogen as fuel in gas turbines can deteriorate the mechanical properties of Ni-based superalloys [11-14]. Because hydrogen permeates to the surface of a specimen by electrochemical hydrogen charging [15,16], the geometry of a specimen may affect the sensitivity to hydrogen embrittlement. In Ni-based alloys, various studies on test conditions such as test temperature, strain rate, and heat treat conditions have been conducted [13,14], but studies on hydrogen embrittlement according to the specimen geometry have not been conducted. To understand hydrogen embrittlement on Ni-based superalloys, Haynes 617 and Hastelloy X alloys with different specimen geometries were electrochemically hydrogen charged, and then a slow strain-rate test (SSRT) was conducted to compare their sensitivities to hydrogen embrittlement in terms of specimen geometry.

2. Experimental

Two Ni-based superalloys of Haynes 617 and Hastelloy X alloys obtained from the JCP Corporation were used in this study. The chemical compositions of these alloys are listed in TABLE 1. After the specimens were mechanically polished and etched by aqua regia (HCl:HNO$_3$ solution at a 3:1 volume ratio) for 30 s, the microstructures were observed using optical

[1] SEOUL NATIONAL UNIVERSITY OF SCIENCE AND TECHNOLOGY, DEPARTMENT OF MATERIALS SCIENCE AND ENGINEERING, 232 GONGNEUNG-RO, NOWON-GU, SEOUL 01811, REPUBLIC OF KOREA

* Corresponding author: bhwang@seoultech.ac.kr

142

Chemical composition of the Haynes 617 and Hastelloy X alloys (wt.%)

Specimen	Ni	Cr	Fe	Mo	Co	Mn	Si	Ti	W	Al	Cu	C
Haynes 617	Bal.	21.9	0.7	9.4	12.3	0.1	0.5	0.3	—	1.4	—	0.1
Hastelloy X	Bal.	22.6	18.1	8.6	1.0	0.4	0.4	0.1	0.8	0.3	0.1	0.1

microscope and scanning electron microscope (SEM; model; EVO10, Carl Zeiss, Germany).

The two types of tensile specimens with different geometries for the Haynes 617 and Hastelloy X alloys were prepared in the rolling direction. The specimen geometries are shown in Fig. 1. The ASTM G142 standard and two-step dog-bone (TSDB) specimens [17] were used to investigate the effect of specimen geometry on hydrogen embrittlement. Some of the tensile specimens were electrochemically hydrogen-charged in an aqueous solution of 3 wt.% NaCl and 0.3 wt.% NH_4SCN with a current density of 500 Am^{-2} for 24 hr using Pt wire as a counter electrode. The SSRT was conducted under a strain rate of 5.0×10^{-5} s^{-1} at room temperature using a universal testing machine with a capacity of 10 tons (model: UT-100E, MTDI, Korea). The specimens before and after hydrogen charging are referred to herein as "Non-charged", and "H-charged", respectively. Following the tensile test, fractured tensile specimens were observed using a SEM.

3. Results and discussion

The OM and SEM images of the Haynes 617 and Hastelloy X alloys are shown in Fig. 2. The microstructures of the alloys exhibited a fully austenite phase with annealing twins, and the grain sizes of the alloys were measured as 118.5 ± 5.1 μm and 66.2 ± 3.2 μm for the Haynes 617 and Hastelloy X alloys, respectively. Some Cr-rich $M_{23}C_6$ precipitates were observed at the grain boundaries of the Haynes 617 alloy, which can cause brittleness under aging conditions [18,19].

Fig. 3 shows the engineering stress strain curves obtained from the SSRT before and after electrochemical hydrogen charging for the Haynes 617 and Hastelloy X alloys. In the non-charged condition, the Haynes 617 alloy exhibited a similar tensile strength and higher elongation as compared with the Hastelloy X alloy. However, the tensile properties varied depending on the specimen geometry under the H-charged condition. No change in elongation was observed after hydrogen charging
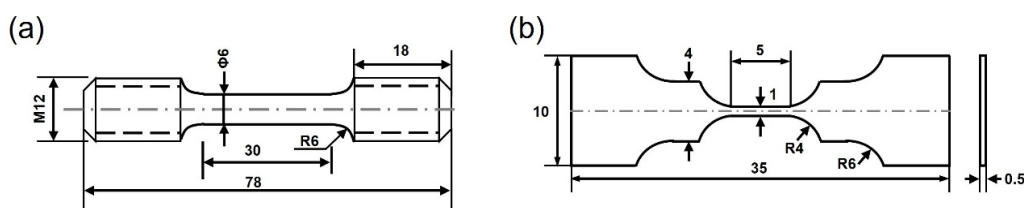

Fig. 1. Specimen geometry for the slow strain-rate test (SSRT); (a) ASTM G142 standard specimen, and (b) two-step dog-bone (TSDB) specimen
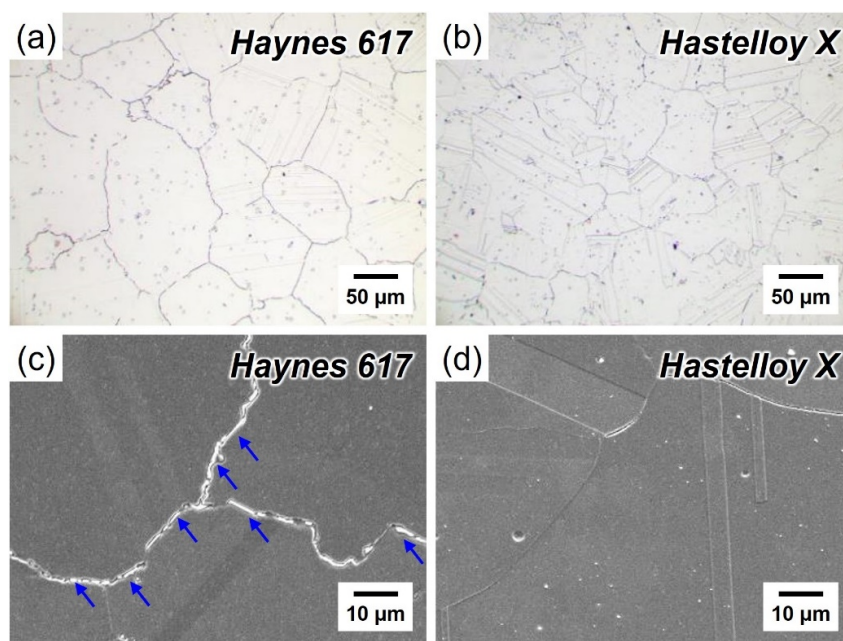

Fig. 2. (a) and (b) Optical microscope (OM) and (c) and (d) scanning electron microscope (SEM) micrographs of the Ni-based superalloys: (a) and (c) Haynes 617 alloy and (b) and (d) Hastelloy X alloy. The blue arrows indicate the presence of precipitates at grain boundaries of the Haynes 617 alloy. The grain size of the Haynes 617 and Hastelloy X alloys was measured to be 118.5 ± 5.1 μm and 66.2 ± 3.2 μm, respectively
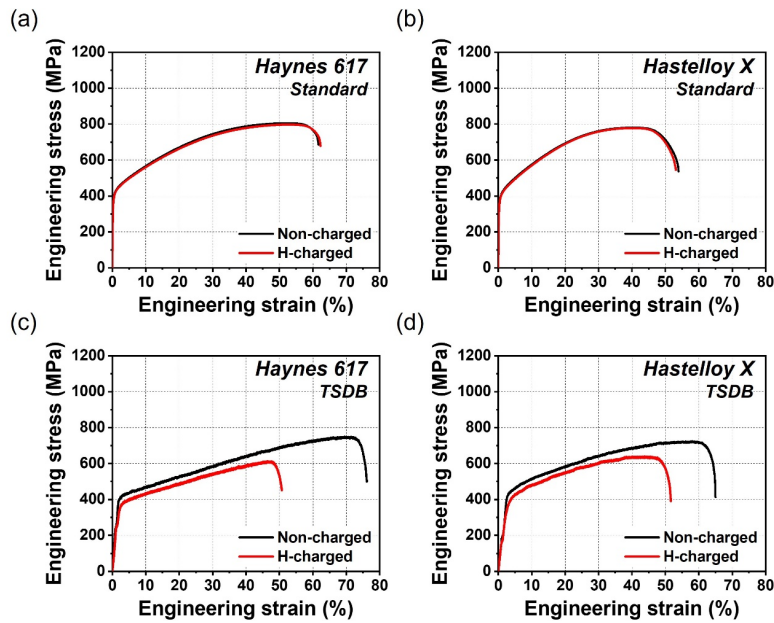
Fig. 3. Engineering stress-strain curves of the (a) and (c) Haynes 617 alloy and (b) and (d) Hastelloy X alloy before and after electrochemical hydrogen charging and according to specimen geometry: the (a) and (b) standard and the (c) and (d) two-step dog-bone (TSDB) specimens. The specimens before electrochemical hydrogen charging were marked as 'Non-charged', and the specimens after electrochemical hydrogen charging were referred to as 'H-charged'

with the standard specimens, whereas the elongation slightly decreased after hydrogen charging with the TSDB specimens. This decrease in elongation was attributed to the fact that the TSDB specimen was more sensitive to hydrogen embrittlement due to its higher surface-area-to-volume ratio. Therefore, it exhibited a higher amount of hydrogen per unit volume of charge [20,21].

On the other hand, the Haynes 617 alloy exhibited lower elongation than the Hastelloy X alloy under H-charged conditions. The different degrees of degradation in elongation could be related to the presence of Cr-rich precipitates at grain boundaries, as shown in Fig. 2. As the Haynes 617 alloy absorbed and trapped more hydrogen than did the Hastelloy X alloy due to the presence

of these precipitates, the increased concentration of hydrogen could promote dislocation nucleation at precipitate-decorated grain boundaries and thus facilitate dislocation slip during deformation [22]. In addition, the Haynes 617 alloy has a coarser grain size as compared with the Hastelloy X alloy. In our study, this resulted in an increase in the grain boundary area, which caused the diffusible hydrogen trapped in the grain boundary to be distributed less effectively and increased the amount of diffusive hydrogen per unit length of the grain boundary [23,24].

Fig. 4 shows fractographs of the TSDB specimens of the Haynes 617 and Hastelloy X alloys before and after electrochemical hydrogen charging. Both alloys in the non-charged
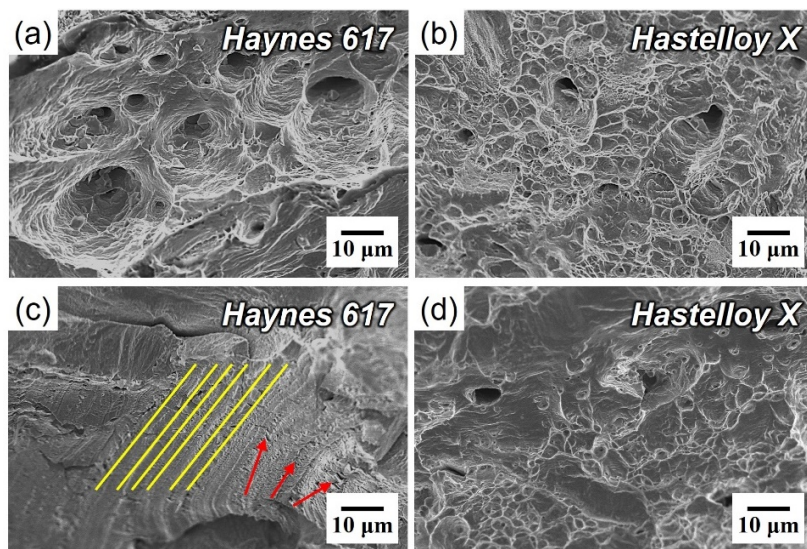

Fig. 4. Scanning electron microscope (SEM) fractographs of (a) and (b) non-charged specimen, and (c) and (d) hydrogen-charged specimen for two-step dog-bone (TSDB) specimens of the Haynes 617 and Hastelloy X alloys. The yellow lines indicate the slip band, and the red arrows indicate the microvoids and crack in the Haynes 617 alloy

specimens displayed a ductile fracture mode with dimples, whereas the fractographs of the H-charged specimens showed different fracture modes. The H-charged specimens of the Hastelloy X alloy exhibited a mixed failure mode including both brittle and ductile fracture, whereas the Haynes 617 alloy did a brittle fracture mode with some cracks initiated from the slip band. The presence of hydrogen can promote slip planarity, leading to high stress concentration at the slip bands. Then, the stress concentration and strain discontinuities at the intersections of the dislocation at slip bands can attract hydrogen [25,26]. The formation and coalescence of microvoids at these sites of local plastic instability, such as at the intersections of slip bands, can induce primary transgranular cracking [27,28].

4. Conclusions

This study investigated the hydrogen embrittlement behaviour of the Haynes 617 and Hastelloy X alloys using the electrochemical hydrogen charging under different specimen geometries. The following conclusions were drawn.

1) Hydrogen atoms were distributed mostly on the surface area during electrochemical hydrogen charging, which caused the two-step dog-bone (TSDB) specimen with a higher surface-area-to-volume ratio to become more susceptible to hydrogen embrittlement as compared with the ASTM standard specimen.

2) The Haynes 617 alloy had a lower hydrogen embrittlement resistance than the Hastelloy X alloy under hydrogen-charged conditions due to its coarser grain size and the presence of precipitates at grain boundaries.

3) In the hydrogen-charged specimens, the Haynes 617 alloy primarily showed an intergranular fracture mode with cracks from the slip band, whereas the Hastelloy X alloy exhibited a combination of transgranular and intergranular fracture behavior derived from the formation and coalescence of microvoids at local plastic instability sites.

REFERENCES

[1] A. Poullikka, Renewable Sustainable Energy Rev. **9**, 409-443 (2005).

[2] S.Y. Lee, S.I. Lee, J. Han, B. Hwang, Mater. Sci. Eng. A **711**, 22-28 (2019).

[3] S. Omano, M. Cerutti, G. Riccio, A. Andreini, C. Romano, J. Eng. Gas Turbines Power **141**, 114501 (2019).

[4] S.I. Lee, S.W. Lee, S.G. Lee, H.G. Jung, B. Hwang, Met. Mater. Int. **24**, 1221-1231 (2018).

[5] Superalloys for gas turbine engines, Introduction to Aerospace Materials **12**, 251-267 (2012).

[6] S.I. Lee, S.Y. Lee, B. Hwang, Mater. Sci. Eng. **742**, 334-343 (2019).

[7] T. Neeraj, R. Srinivasan, J. Li, Acta Mater. **60**, 13-14 (2012).

[8] K. Park, D.H. Cho, M.H. Park, C.W. Yang, Kor. J. Met. Mater. **57**, 405-411 (2019).

[9] P. Gobbato, M. Masi, A. Toffolo, A. Lazzaretto, Int. J. Hydrog. Energy **36**, 7993-8002 (2011).

[10] E. Ma, S. Park, H. Choi, B. Hwang, J. Byun, J. Powder Mater. **30**, 217-222 (2023)

[11] F. Lecoester, J. Chêna, D. Noel, Mater. Sci. Eng. A **262**, 173-183 (1999).

[12] T.W. Hong, S.I. Lee, J.H. Shim, M.G. Lee, J. Lee, B. Hwang, Met. Mater. Int. **27**, 3935-3944 (2021).

[13] Z. Zhang, K.L. Moore, G. McMahon, R. Morana, M. Preuss, Corros. Sci. **146**, 58-69 (2019).

[14] A. Nagao, K. Hayashi, K. Oi, S. Mitao, ISIJ Int. **52**, 213-221 (2012).

[15] Z. Wang, M. Huang, Metals **10**, 1585 (2020).

[16] R. Karmakar, P. Maji, S.K. Ghosh, Met. Mater. Int. **27**, 2134-2145 (2021).

[17] D. Wang, X. Lu, D. Wan, X. Guo, T. Johnsen, Metall. Mater. Trans. A **802**, 140638 (2021).

[18] X. Lu, Y. Ma, D. Wang, Mater. Sci. Eng. A **792**, 139785 (2020).

[19] T.S. Jo, J.H. Lim, Y.D. Kim, J. Nucl. Mater. **406**, 360-364 (2010).

[20] D.P. Escobar, C. Miñambres, L. Duprez, K. Verbeken, M. Verhaege, Corros. Sci. **53**, 3166-3176 (2011).

[21] X. Lu, D. Wang, D. Wan, Z. B. Zhang, N. Kheradmand, A. Barnoush, Acta Mater. **179**, 36-48 (2019).

[22] A. Aghajani, J. Tewes, A.B. Parsa, T. Hoffmann, A. Kostka, J. Kloewer, Metall. Mater. Trans. A **47**, 4382-4392 (2016).

[23] C. Park, N. Kang, S. Liu, Corros. Sci. **128**, 33-41 (2017).

[24] H. Yang, T.T. Nguyen, J. Park, H.M. Heo, J. Lee, U.B. Baek, Y.K. Lee, Met. Mater. Int. **234**, (2022).

[25] M. Sundararaman, P. Mukhopadhyay, S. Banerjee, Acta Metall. **36**, 847-864 (1988).

[26] R. Kirchheim, Acta Mater. **55**, 5129-5138 (2007).

[27] V. Demetriou, J.D. Robson, M. Preuss, R. Morana, Int. J. Hydrog. Energy **42**, 23856-23870 (2017).

[28] S.I. Lee, J. Lee, B. Hwang, Mater. Sci. Eng. A **758**, 56-59 (2019).